# A Photovoltaic Sourced Buck-Boost Converter Design with a Robust Sliding Mode Control

**Mustafa Ergin Şahin[*1], Halil İbrahim Okumuş[2] and Hakan Kahveci[2]**

[1]Department of Electrical and Electronics Engineering, Recep Tayyip Erdoğan University, 53100 Rize, Türkiye, e-mail: mustafa.sahin@erdogan.edu.tr

[2]Department of Electrical and Electronics Engineering, Karadeniz Technical University, 61080 Trabzon, Türkiye, e-mails: okumus@ktu.edu.tr, hknkahveci@ktu.edu.tr

[*]Corresponding author

*Abstract: A sliding mode controller (SMC) for a photovoltaic (PV)-powered DC to DC buck-boost converter to supply a constant load voltage is investigated in this paper. The indirect method is used to adjust the PV source to its maximum power point by the converter and SMC. This study presents SMC without using system dynamics, models, and transfer functions as an effective and easily adjusted controller. The PV source and battery loads behave differently from linear sources and require a robust controller to accommodate various loads and PV conditions. Compared with classical PI/PID and non-sliding nonlinear controllers, SMC provides better disturbance rejection, finite-time convergence, and independence from exact model parameters. These advantages are essential for PV-powered converters, where voltage levels vary continuously. The PV-powered converter and SMC system were simulated for these conditions. Also, the setup was implemented using the digital signal processor (DSP) TMS320F28335 to verify the proposed idea and simulation results. The inductance current variation and the load voltage of the converter were used as control variables for the SMC. The system's performance was investigated for different voltage variations of the converter, and simulated using different reference voltage values with the PV module as a voltage source. Total harmonic distortions (THD) for the converter were also investigated. The effects of voltage variations were observed, and the results were compared for the stability analyses. For the stability of the whole system, the Lyapunov stability analysis was used in this study. The mathematical equations to supply these criteria are given with the small signal analysis method. The simulation and experimental results overlapped with the theoretical expectation. The performance of the DSP in processing the SMC algorithm using the current and voltage feedback signals was observed experimentally.*

*Keywords: buck-boost converter; digital signal processing; nonlinear control; PV source; sliding mode control*

# 1 Introduction

One of the PV system's main problems is adjusting the system output for a constant load or bus voltage [1]. The DC-to-DC converters must be used to adjust the output voltage generated by the PV systems [2]. The PV sources and battery loads are composed of nonlinear system parts [3]. The automatic control of such a complex nonlinear PV battery storage system is not easy for conventional controllers [4]. SMC was proposed for stability and implemented as a robust and easy-adjusted controller independent of system dynamics.

Photovoltaic sources have some different properties from other linear power sources [5]. Design and implementation are required for modelling the PV model as a nonlinear and limited power source [6]. PV array models are used as a source in actual PV panels [7]. A PV module model has been designed to obtain the necessary power by combining the PV cells used in previous studies [8] [9].

This paper offers the designed experimental setup of the buck-boost converter and the other feedback control circuits with the DSP controller [10]. The realized buck-boost converter is controlled using TMS320F28335 coded eZDSP (Manufactured by Spectrum Digital Corporation) for the PV-powered experimental setup [11]. The converter output voltage and inductance current variations are measured and processed as SMC variables by the DSP's analog-to-digital converter (ADC) [12-13]. The suggested PV-powered converter topology is simulated using SMC in MATLAB/Simulink [14]. SMC for switching power supplies is a control system that works for a switching hysteresis band [15] [16]. A method known as an indirect control method is used for the maximum power point tracking (MPPT) of the PV module model. This indirect method is defined using the PV panel datasheet characteristics in MPP voltage [17]. Generally, this MPP voltage is selected as a converter reference output voltage in basic applications [18]. The authors have applied and validated this indirect method for different controllers in their previous works instead of traditional MPPT control methods [17] [19].

Some traditional methods in the literature are used for the control of converters [20]. Although these controllers were previously used as a solution for applications, they are not sufficient now to solve the problems of the controllers with nonlinear sources and loads [21]. If the converter is a simple voltage converter, it is suitable to use a proportional-integral (PI) controller. However, it cannot be sufficient to control some nonlinear systems alone without an adaptive controller [22].

The main advantage of SMC is that it is suitable for variable structure systems control since it does not need to calculate control parameters like the PID controller [23]. The SMC is developed for a nonlinear controller's need for switching power supplies, such as a DC/DC buck, boost converter [24-27]. Strong dynamic response and easy implementation with microcontrollers are some of the advantages of SMC [28]. Moreover, the trajectory of the system moves in a defined area. This area is defined as a sliding surface for the SMC on the specific state space. The SMC for

switching power supplies works in a switching hysteresis band [15]. There are some advantages compared to different control methods in the literature [19, 29, 30].

For the boost types, DC to DC converter PWM-based SMC are modelled and simulated in MATLAB/Simulink software, and the efficiency of SMC and PI controllers is compared in a study [31]. The response of a boost-type DC to DC converter is analyzed with MATLAB/Simulink software using SMC and a PV source, and the transient response of the boost converter output is seen as superior to the PI controller [32]. The SMC is proposed in another work to keep and stabilize the DC bus voltage constant by controlling the converter. Also, the simulation results of PI and PID controllers are compared with the SMC results. The SMC decreases the steady-state error of the output voltage, catching the transient response better [33]. In another study, the robotic manipulators' trajectory tracking control based on the model-free PID-SMC method is presented. This control scheme combines the superior properties of the PID controller and SMC [34]. A grid-connected PV system's automatic voltage regulation has been investigated using a Lyapunov-based SMC, in another study. Better and higher efficiency of the offered SMC is observed and compared with the PI controller, and details are given in the simulations [35].

Performance estimation of a low-power SMC buck-boost converter for different control laws has recently been investigated in a study with limited results [36]. The simulation of the buck-boost converters has been proposed using PI, SM, and Fuzzy Logic Control (FLC) in MATLAB/Simulink currently. Also, the SMC theory is given in more detail in the referred paper [37]. An efficient solar-hydrogen DC-DC buck converter system with SMC is proposed for electrolysis load as well [38]. An SMC strategy with DC capacitor voltage balancing is proposed and offers dynamic performances and excellent steady-state with low THD in another study [39]. The stability of three-phase LCL-filtered grid-connected voltage source inverters improved by observer-based SMC is used in another paper [40]. The motor driver application of SMC is first presented for a converter in a thesis [41].

It is possible to find some different applications of SMC in literature, super-twisting sliding mode control structures [42], improving value-based reinforcement learning with control applications [43], sliding mode control using adaptive fuzzy system under constrained input amplitude [44], a piecewise Lyapunov functional is established to analyse the exponentially stable of the switched system [45], another paper proposes a quadratic prescribed performance function design [46], at last a paper proposes to mix two data-driven algorithms [47].

Although numerous studies have focused on SMC for power converters, the literature still lacks a unified perspective addressing PV-powered buck–boost converters operated under wide disturbances and nonlinearities. Prior research mainly investigates classical SMC structures, SMC–PI hybrids, fuzzy-SMC strategies, and Lyapunov-based SMC approaches. However, studies that combine indirect MPPT operation with a fully DSP-embedded SMC implementation remain

limited. Therefore, this work aims to fill this gap by providing a complete theoretical, simulation-based, and experimental evaluation of SMC applied to PV-powered converters under variable irradiation and voltage conditions. An experimental system in literature was implemented for the first time in this paper, with more details for these conditions, which will be useful for scholars in this area.

The motivation of this study arises from the need for a robust, model-independent, and DSP-practical controller capable of maintaining stable output voltage despite severe PV fluctuations. This paper offers the designed experimental setup of the PV-powered buck-boost DC to DC converter and the other supplementary circuits with the DSP controller. The suggested PV-powered converter system is simulated in MATLAB/Simulink software using SMC for all inrush and nonlinear conditions and THD. The realized buck-boost converter is controlled using TMS320F28335 coded eZDSP for the PV-powered experimental setup for real-time and fast control. The converter output voltage and inductance current variations are measured and processed as SMC variables with the designed circuits. The simulation and experimental results are compared for different variables to verify and increase the reliability of this new idea in power converters.

# 2 The Calculation of the Converter Parameters

The suggested DC-DC buck-boost converter for the nonlinear photovoltaic source and constant load's voltage with the SMC is seen in Fig. 1. To obtain the voltage error, the converter output or load voltage ($V_o$) is compared with the desired voltage reference ($V_{ref}$) value. This voltage of error is applied to the SMC to compare it with the inductance current value to assign the duty cycles of switching PWM signals [14]. The obtained switching signal drives the converter's switching MOSFET. All these processes are performed with a DSP on the implemented setup.

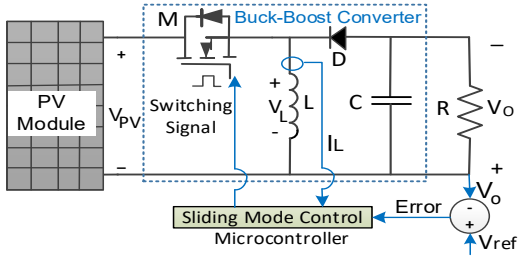


Figure 1

PV-powered converter circuit with an SMC control block

The basic buck-boost converter and current flow for the two-state system are shown in Fig. 2(a). When the switching signal is high-level, the current flows over the MOSFET and the inductance component. When the switching signal is turned off,

the inductance current continues to flow over the load, capacitor, and diode components. If the inductance value is enough to continuously supply the load and not go to zero, it is called continuous conduction mode (CCM) for the converter. The efficiency of converters depends on the inductance current value for the converter in CCM. The converter's working mode is determined by the inductance value under different load conditions. The converter's inductance voltage and currents are changed by switching the PWM signal for CCM, as seen in Fig. 2(b).

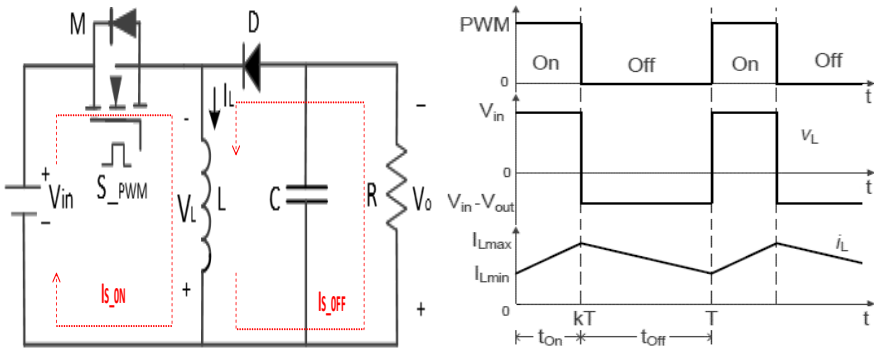


(a) (b)

Figure 2

Buck-boost converter currents for two-state (a), Inductance voltage, and current variation with PWM signal at the CCM (b)

The suggested converter system is planned for a constant bus voltage value. Therefore, a variable PV voltage is transformed into a fixed output voltage by the DC-to-DC buck-boost converter for several resistance loads. The converter circuit is planned for 200 Watt PV panel power, 37.5 kHz PWM frequency, and less than 1% voltage regulation at the output.

The converter setup is investigated for the duty ratio ($D$) of the switching signal, which changes between 0 and 1. The converter works in the buck mode if the $D$ value is between 0 and 0.5; otherwise, it works in the boost mode. The maximum input power of the converter ($P_{in}$) is calculated for the MPP of PV panel as in (1).

$$P_{in}=V_{in}\times I_{in}=24\times 8.33=200\ Watt \tag{1}$$

The converter efficiency ($n$) is accepted at 90% according to the traditional converters, and the output power ($P_O$) is calculated as in (2).

$$n=\frac{P_o}{P_{in}} \Rightarrow P_o = 180\ Watt \tag{2}$$

The output current ($I_O$) is calculated as in (3) for the converter's expected output voltage and power.

$$I_o = \frac{P_o}{V_o} = \frac{180}{24} \Rightarrow I_o = 7.5\ A \tag{3}$$

The output load resistance ($R$) is calculated as in (4).

$$R = \frac{V_o}{I_o} = \frac{24}{7.5} \Rightarrow R = 3.2\ \Omega \tag{4}$$

The minimum value of inductance ($L$) is found using in (5), which is derived from the current ripple of inductance for switching frequency ($f$) and the $D$=0.5 [10].

$$L=\frac{R(1-D)^2}{2f}=\frac{3.2\times0.25}{2\times37.5\times10^3}=10.5\ \mu H \tag{5}$$

The minimum capacitor *(C*) value under the 1% output voltage ripple ($\Delta V_O$) and for $T_S$=3 msec switching period is found using (6).

$$\frac{\Delta V_O}{V_O}=\frac{D\times T_S}{R\times C}\Rightarrow\frac{0.24}{24}=\frac{0.5\times0.03\times10^{-3}}{3.2\times C}\Rightarrow C=480\ \mu F \tag{6}$$

These critical inductance and capacitor values are necessary for simulations and experimental parts to use the converter in CCM and for a minimum voltage ripple. The closed-circuit state equations obtained from Figure 2(a) are written as a matrix form in (8) using the circuit parameters in (7) for the transfer function of the converter:

$$\begin{aligned} x_1 &= i_L \\ x_2 &= V_C \rightarrow \dot{x}_2 = \frac{dV_C}{dt} \end{aligned} \tag{7}$$

$$\begin{bmatrix} \dot{x}_1 \\ \dot{x}_2 \end{bmatrix} = \begin{bmatrix} \frac{r_C(d+1)-r_L}{L} & \frac{1}{L}(d-1) \\ \frac{1}{C}(d-1) & \frac{1}{RC}(2d-1) \end{bmatrix} \begin{bmatrix} x_1 \\ x_2 \end{bmatrix} + d \begin{bmatrix} \frac{1}{L} \\ 0 \end{bmatrix} V_{in} \tag{8}$$

The transfer function of the DC to DC converter can be simplified as in (9). The details of these calculations can be found in the referred study [19].

$$\frac{\hat{V}_0(s)}{\hat{d}(s)}=\frac{V_{in}}{(1-d)^2}\frac{(1+\frac{s}{1/r_C C})(1-\frac{s}{(1-d)^2 R/dL})}{\frac{s^2}{(1-d)^2/LC}+\frac{s}{(1-d)^2 R/L}+1} \tag{9}$$

The obtained and calculated values of the converter; $V_{in}$ = 24 V, $r_C$ = 0, $r_L$ = 0, C = 480 µF, L=10.5 µH, and R = 3.2 Ω are written in (9) for the duty ratio (D) of 0.5, and the transfer function is found numerically as in (10):

$$\frac{\hat{V}_0(s)}{\hat{d}(s)}=\frac{24-31.5\times10^{-4}s}{5.4\times10^{-9}s^2+3.28\times10^{-6}s+0.25} \tag{10}$$

The Bode diagram of (10) is plotted in MATLAB/Simulink as in Figure 3. The phase and magnitude variations with frequency indicate that the system does not supply the stability conditions because phase margin is -89.2 deg. and gain

margin is -59.6 dB, and an error amplifier is required as a compensator to stabilize the system.

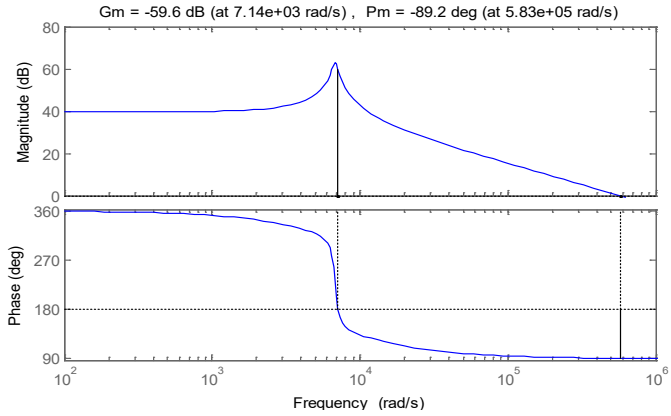


Figure 3
The Bode diagram for the open-loop transfer function of the buck-boost converter

# 3 The Sliding Mode Control Theory for Converters

As the field of SMC applications increases, many researchers have searched for the implementation of SMC in electromechanical systems lately [2]. The main areas where the SMC method has been applied are overviewed for control details in Table 1.

Table 1
SMC applications overview in electromechanical systems

| Applications | SMC Methods Details | References |
|---|---|---|
| Motor drivers | SMC, Fuzzy SMC, Continuous SMC | [15] [51] [52] |
| Robot applications | PID+SMC, Optimal SMC, Fuzzy NN | [34] [52-57] |
| Nuclear, Mechatronic | SMC and Fuzzy Adapted SMC | [44] [58] [59] |
| Aircraft, motor torque | MIMO SMC, Nonlinear position control, | [48] [60] |
| AC-DC rectifiers | Observed based on SMC | [39] [40] [61] [62] |
| DC-DC converter (Related case study) | SMC for converters, Robust SMC, DSP-based SMC, PID, FLC comparison, | [1-4] [14] [24-33] [36-38] |
| PV Energy and Wind applications | Lyapunov-based SMC, Integral SMC for MPPT, PSO-based SMC for P&O MPPT | [21] [35] [49] [50] [63] [64-67] |
| Tank system | Super twist SMC | [42] |

The SMC controls switching mode power supplies (SMPS), which have nonlinear input and output variables extracted from the variable structure controllers.

The increasing use of renewable energy sources in the electronics industry and the widely varying loads supported only by power converters using a nonlinear controller make it compulsory to understand this process. The easy application, effective error control, and dynamic response are advantages for high load variations proposed by SMC [30].

The SMC proposes a solution for variable structure systems, and state variables control the converter switches in practice. This controller forces the system trajectory to stay in a state space area, which is known as a sliding surface. The state equation is given for a single-input and piecewise classified nonlinear system in (11), where the control rule is also defined. The equation parameters are the scalar control input ($u$) on the sliding surface, in which $s(x, t)=0$ is a transient vector, and $f(x)$ and $g(x)$ are known as continuous function vectors which are used as output voltage and inductance currents of a converter as state variables.

$$\dot{x}=f(x,t)+g(x,t)u,\ u=\{0,1\} \tag{11}$$

State trajectories that have a dynamic action and slide into a balanced line asymptotically for the SMC. Defining the control rule to specify the sliding surface for the controller's $s(x)$ is critical in this method. The other important point is that state trajectories hold onto the system's switching surface for the power converters. The Lyapunov method is selected to design this controller in this study [16]. SMC laws are not continuous and can drive trajectories to the SM for an infinite time. Lyapunov stability analysis is used in this study for the stability of the system.

The system acts as an SM when the trajectories arrive at the sliding surface, and the origin $s=0$ may only have asymptotic stability there. The SMC switching function ($\sigma$) is represented as a distance from a sliding area. If state $x$ is outside of this sliding surface, the switching function has $\sigma(x)\neq 0$, else a state is on this sliding surface, the switching function has $\sigma(x)=0$. Depending on the sign of this distance, the SMC switches from one state to another. So, the SMC is always forced in the direction of the sliding mode where $\sigma(x)=0$ [41] [48].

The state trajectory ($s$) is expected to move in the defined surface for optimum SMC, probably with an unlimited switching frequency [49]. However, switching frequency is limited to a calculated value in virtual systems. This switching frequency makes some oscillations called fluctuations on a switching surface [19]. The system trajectory and sliding surface are shown in Figure 4.

The system trajectory stays on the sliding surface under the SMC, and it is described in Equations (12) and (13), as shown in Fig. 4 [2]. The switching function is defined as in Equation (12), where $c$ is a plus design coefficient, and the centerline in Fig. 4 represents the set of points for the equation [41].

$$s(x,\dot{x}) = cx + \dot{x} \ \rightarrow \dot{s}(x,\dot{x}) = 0 \ \rightarrow \dot{x}(t) = -cx(t) \tag{12}$$

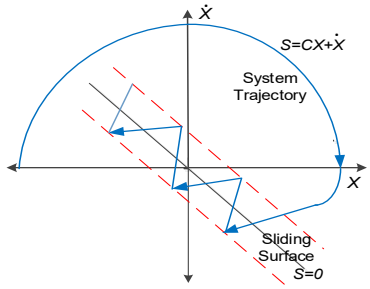


Figure 4
System trajectory moves towards the sliding surface for SMC [19]

$$\dot{s}(x,t)=\frac{ds}{dt}=\sum_{i=1}^{n}\frac{\partial s}{\partial x_i}\frac{dx_i}{dt}=\nabla s\,\dot{x}=G\dot{x} \tag{13}$$

$G$ is a 1-*by*-$n$ matrix, and the elements of this matrix are derived from the sliding surface. Equation (14) is obtained using (11) and (13). Instead of control input ($u$), use equivalent control input ($u_{eq}$) in (14), which defines the system variation on the sliding surface.

$$G\dot{x}=Gf(x,t)+Gg(x,t)u_{eq}=0 \tag{14}$$

$$u_{eq}=-(G\,g)^{-1}G\,f(x,t) \tag{15}$$

Equation (15) was substituted into (11) and obtained (16):

$$\dot{x}=f(x,t)-g(x,t)(G\,g)^{-1}f(x,t) \tag{16}$$

Equation (17) is a state equation and defines the system movements for SMC, where $u_{eq}$ is an equivalent vector, and $G$ is an $m$ by $n$ matrix.

$$\dot{x}=\left[I-g(x,t)(G\,g)^{-1}G\right]f(x,t) \tag{17}$$

From Equation (12), the control law in (18) is selected:

$$u=\{0\ \ for\ \sigma(x)>0\ 1\ for\ \sigma(x)<0\} \tag{18}$$

The state equations are written as below in (19), which involves the output error and its derivative [2, 3, 50]:

$$\dot{x}=\ Ax+Bu+D \tag{19}$$

Equation (20) can be written using (12):

$$\dot{\sigma}(x)=C^T\dot{x}=0 \tag{20}$$

Where $C^T = [c_1, 1]$ is the vector of the sliding surface coefficient. It corresponds to $G$ in (13). The coefficient $c_2$ is set to one. Equations (19) and (20) are combined and written as in (21):

$$\dot{\sigma}(x) = C^T Ax + C^T Bu + C^T D \tag{21}$$

For the control law in (18), (21) is written as in (22):

$$\dot{\sigma}(x) = \begin{Bmatrix} C^T Ax + C^T Bu^+ + C^T D < 0 \; for \; \sigma(x) > 0 \\ C^T Ax + C^T Bu^- + C^T D > 0 \; for \; \sigma(x) < 0 \end{Bmatrix} \tag{22}$$

Locating the obtained matrixes (A, B, D) from the state (19) into (22) obtained the two-line Equations to define a sliding surface region. In these surfaces, the $c_1 > 1/R_L C$ or $c_1 < 1/R_L C$, and the $k$ value in Figure 5 is $k = c_1.R_L C$ and after the simulation results, the $k$ value is obtained as 1 for the best result [2, 38, 41]. In practice, the Lyapunov function coefficients were selected by considering converter response time, ripple constraints, and DSP sampling limitations. A higher $c_1$ improves convergence speed but increases switching activity; therefore, $c_1 = 1/R_L C$ was found to provide an optimum trade-off between robustness and efficiency

Another property of SMC is that the system response is obtained without system parameters. Therefore, SMC is appropriate for DC-to-DC converters. The speed of the current variation for converter practices is faster than the speed of the output voltage variation. This property is applied to the control method by using an internal nonlinear inductance current control loop and an external nonlinear voltage control loop for the output. These two control loops create the SMC. Therefore, the standard linear voltage controller is used as an outer loop for the output voltage value control. A hysteresis mode controller is used for the nonlinear inductance current variation controller as an inner loop. The SMC principle for the converter's general structure is seen in Figure 5 and simulated with a MATLAB/Simulink model, and performed with a microcontroller experimentally.

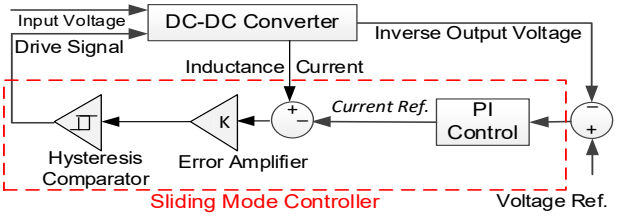


Figure 5

The basic principle of the SMC for the DC to DC converter [3, 38]

The computational complexity of the proposed SMC algorithm is low, as it primarily consists of sign-based switching logic and linear operations for the sliding surface evaluation. Unlike model-based controllers, the method does not require online parameter estimation or matrix inversion. The DSP TMS320F28335 executes the algorithm within a single switching cycle (37.5 kHz), indicating that the computational burden is negligible for real-time implementation.

# 4 The PV-powered Buck-Boost Converter Model

The converter model is developed visually in MATLAB/Simulink software with SMC in this section, and basically, the converter model is represented in Figure 6. The output voltage is compared with the reference voltage, and a voltage signal error is obtained in the first feedback. The reference current signal is provided by an integrator when the error value of the voltage signal is applied to a linear voltage controller in the second feedback. The switching MOSFET is driven by the PWM signal, where currents are applied to a hysteresis relay controller [2, 15, 21]. The SMC algorithm, seen in Figures 5 and 6, is described in Equation (23). The $K_1$ and $K_2$ control parameters are used to fine-adjust switching signals obtained using this study's trial-and-error method.

$$Switching\ Signal = K_2 (I_L - K_1 \int (V_{ref} - V_O)) u,\ u = \{0,1\} \tag{23}$$

The Lyapunov function is selected such that the sliding surface ensures negative definiteness of its derivative. This guarantees global reachability of the sliding manifold and asymptotic convergence once the trajectories reach s=0. The derived inequalities explicitly show the conditions on the controller gains ($K_1$, $K_2$), which ensure stability under both buck and boost operating modes. The sliding mode existence domain corresponds to the region in which the reachability condition $s \cdot \dot{s} < 0$ holds. For the proposed converter, this domain is bounded by the designed hysteresis band on the inductor current, ensuring that trajectories remain within $\pm\Delta I$ around the sliding surface.

The basic equation of a PV cell depends on the PV parameters given in (24):

$$I = I_L - I_0 \left[ \exp\left(\frac{q(V + R_s . I)}{n.k.T}\right) - 1 \right] - \frac{V + R_s . I}{R_{sh}} \tag{24}$$

Practical PV systems operate under severe irradiation and temperature variations; therefore, the proposed robust control method in Figure 6, which can guarantee stable output voltage without complex tuning, is highly desirable.

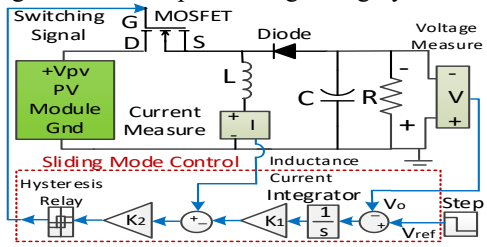


Figure 6
Simulation model of PV-sourced and SMC added buck-boost converter

The voltage of the PV module increases when the PV cells are connected in series. When connected in parallel, the current of the PV module increases. The combining

model is described as a PV module and given for all parameters in (25). The PV and SMC parameters in (23-25) are described in Table 1.

$$V_{PV}=\frac{N_S.n.k.T}{q}\ln\left[\frac{(I_{SC}+K_I(T-T_{ref})).G+I_0-I_{PV}+N_P}{I_0.N_P}\right]-\frac{N_S}{N_P}R_s.I_{PV} \tag{25}$$

The PV module has been described in (25) and simulated in MATLAB/Simulink previously. Therefore, all the parameters and derivation steps of the equation have been found in previous studies [8] [17]. The MATLAB/Simulink model of a PV module derived from (25) is represented in Figure 7 (a). The *I-V* curve of the PV module for 200 W MPP is represented in Figure 7 (b). The *I-V* curve shows that the PV module generates variable voltages between 0 V and 30 V, depending on the current supplied by the PV module. The MPP voltage and current are given in Figure 7 (b). The P-V curve of the simulated PV module for 200 W MPP is illustrated in Figure 7 (c). The MPP voltage is about 24 V, and this is also equal to our converter's output voltage, as in the indirect method [17]. The simulation parameters of the buck-boost converter and PV module are given in Table 2.

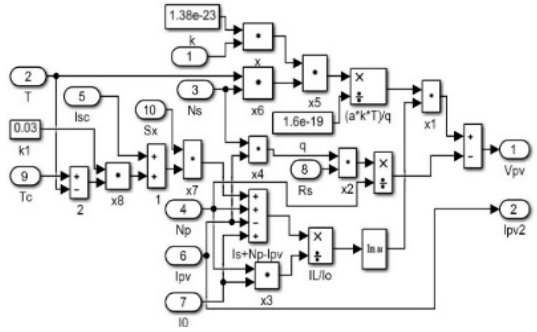


(a)

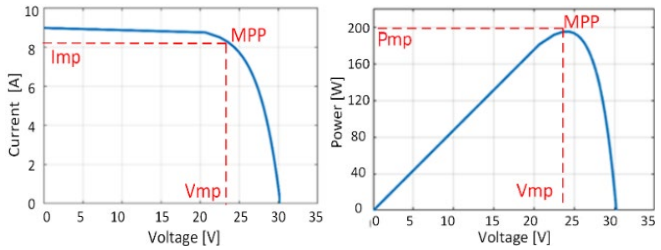


(b) (c)

Figure 7

(a) The PV module MATLAB/Simulink model, (b) Simulation result of I-V curve and MPP, (c) the P-V curve and MPP

Table 2
All the simulation parameters and values

| Simulation Parameters | Simulation Values |
|---|---|
| Variation of PV input voltage | 0 - 30 V |
| PV Maximum Power | 200 W |
| Two reference output voltages | 7 V(Buck ) 14 V(Boost) |
| Converter switching frequency | 37.5 kHz |
| Converter inductance value | 10 µH |
| Converter capacitance value | 5 mF |
| Output load resistance | 3.2 Ω |
| Boltzmann constant (*k*) | $1.38x10\text{-}^{23}$ J/K |
| Electron charge (q) | $1.6x10^{-19}$ C |
| Reference temperature (T) for panel | (273+25) K |
| Short circuit current temp. constant ($K_1$) | 3 mA/ºC |
| Diode current (Io) | 50 µA |
| Short circuit current (Isc) | 3.92 A |
| Series cell number of PV module (Ns) | 50 |
| Parallel cells number of PV module (Np) | 150 |
| Series internal resistance (Rs) | 0.0277 Ω |
| Variable temperature (Tx) | 25 ºC |
| The light absorption (Sx=G) | 1 kW/m² |
| Ideality factor (a=n) | 1.2 |
| SMC proportional gains | $K_1$=10, $K_2$=1 |

# 5 Simulation Results

The DC to DC buck-boost converter simulation results with SMC for different references and 12 V input voltage are illustrated in Figure 8(a). The response of the unit step for several references and how they change with time is represented in the simulation results. The transient response is mainly dependent on the converter circuit's output resistance and capacitor value, which is calculated depending on the switching frequency. Performance specifications are steady-state voltage ripple <1%, overshoot <10%, settling time <30ms, and robustness to ±50% PV voltage variation. This result shows that the converter's output voltage moves from a nonlinear trajectory to the sliding surface limited by the SMC of this surface.

This converter control system aims to fix the variable input voltage around the reference output voltage to be a constant load voltage. The PV voltage is compared with the load voltage as seen in Figure 8(b). The converter is adjusted to approximately 11 V input PV voltage, and it works in boost mode for the first second and buck mode for the last second. The PV source voltage is reduced or

enlarged for different reference voltages. These reference voltages are 14 V for boost mode and 7 V for buck mode, mentioning that the charge voltage of 12 V and 6 V are for the nominal voltage of batteries. For one reference (24 V) and a variable PV source (14 V and 28 V), the simulation result is shown in Figure 8(c). The inductance voltage value and current variation with PWM for boost mode are shown in Figure 8(d). The reference voltage is held on with SMC for every condition, with less ripple. The simulation results show that the SMC theory is compared with the simulation results expected for the designed model.

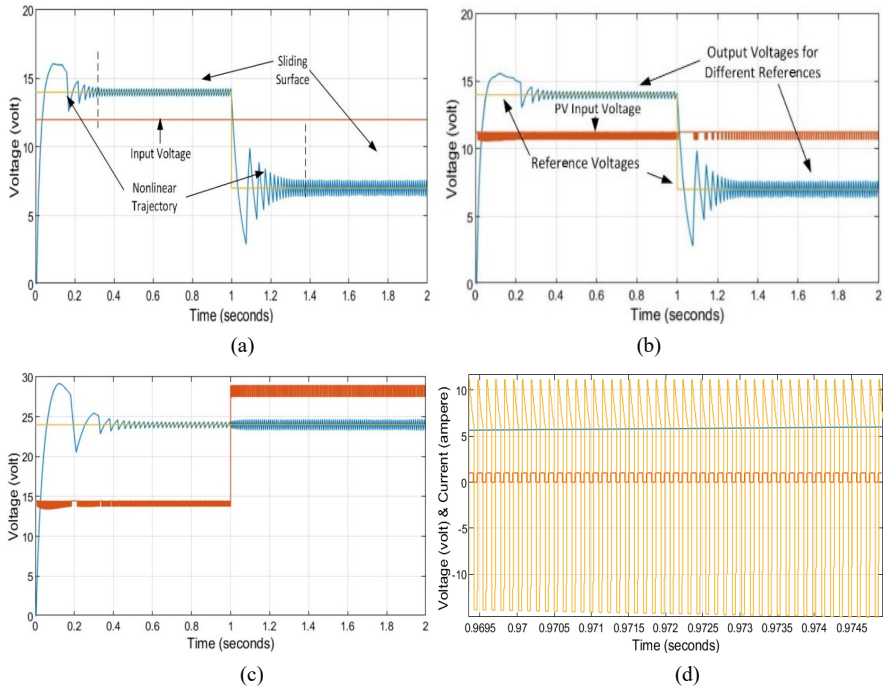


Figure 8

Simulation result of output voltage for two different references (7 V and 14 V) with SMC, (a) For a DC source, (b) For a PV source, (c) For one reference and variable PV source (14 V and 28 V), (d) Inductance voltage and current variation with PWM signal for boost mode

# 6 Experimental Setup and Results

The experimental setup of the converter is designed appropriately for the simulation model. Also, voltage and current measurement circuits have been performed using a voltage transducer (LV 25-P) and a current transducer (LTS 25-N) for the experimental setup. Measurement results are sent to the ADC input of the DSP for processing the data. The used voltage and current measurement LEM transducers

are given in datasheets in more detail [12] [13]. The SMC algorithm is intended to be shown in Figure 5 in the code composer software of DSP, and the obtained switching signal from the PWM outputs of DSP drives the MOSFET.

The required converter circuit and peripheral circuits are experimentally designed. The required voltage value for the switching signal amplitude is increased by the MOSFET driver circuit. Also, the converter's output voltage is limited between 0 and 3.3 V so as not to damage the DSP [11]. The voltage of the measuring and control circuits is supplied by the auxiliary batteries to ensure the uninterrupted operation of the control system. Some circuits, such as voltage dividers, filters and amplifiers, have been designed for this purpose and implemented. The high-frequency switching circuits directly affect measurement signal sensitivity. This experimental setup is seen in detail in Figure 9 (a, b).

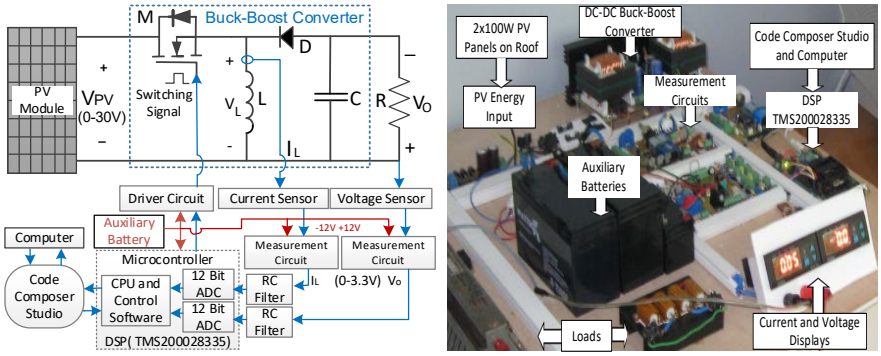


(a) (b)

Figure 9

The block diagram of the experimental setup (a), an image from the setup (b)

The PV source is adjusted to 15 V for buck mode or 30 V for boost mode to work the converter. The experimental result of the output voltage with the input step voltage for the converter buck mode is given in Figure 10(a). The converter's 30 V input voltage in buck mode is decreased to a constant 24 V inverse output voltage. The output response of SMC with input step voltage variation is given for boost mode in Figure 10(b). The converter's 15 V input voltage is increased to a constant 24 V output voltage in boost mode. The converter output voltage tracks the required reference voltage after a few big ripples (10-15 V) in a trajectory and oscillates with a slight fluctuation (0-1 V) on the sliding surface. However, the output voltage of the converter has a long response time, and some small ripples hold the desired voltage reference correctly in two states. The fluctuations at a steady state for the dynamic system are compatible with the simulation results in Fig. 8. The minor differences that occurred depend on a virtual system measurement error, noise, system response, and the absence of simulation results. While a high overshoot and low ripples are seen in buck mode, slight overshoot and high fluctuations are seen in boost mode, depending on inductance current and output voltage.

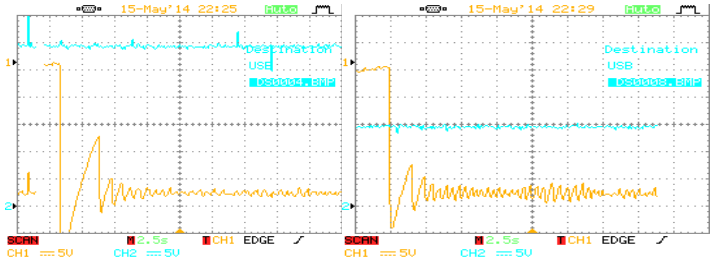


(a) (b)

Figure 10

Change of input (CH2 a, b) and output voltage (CH1 a, b) for Buck (a) and Boost (b) mode

Experimental results are observed with a Tektronix corporation trademark oscilloscope, and a 1 MHz current probe (Pintek corporation trademarks) is seen in Figures 11-13. The DC input and output voltage and inductance current values are illustrated in Figure 11 (a). The converter outputs track the 24 V reference voltage for the 15 V DC input voltage. Also, the inductance current is illustrated in Figure 11 (a) and has some ripples depending on the controller. These ripples arise from the change in the duty ratio. The input and output voltages and the inductance current value changes depending on the duty ratio are presented in Figure 11 (b). The duty ratio of the switching signal changes depending on the variation of the inductance current. Also, it is observed that in Figures 11 and 12, the ripples on PV voltage depend on the switching signals and are eliminated on the converter output voltage depending on the LC components of the converter.

The PV source and output voltage value, and inductance current variations with PWM signals are illustrated in Figure 12 (a) for the boost mode of the converter. The converter outputs track the 24 V reference voltage for the 20 V DC input voltage, and the output voltage oscillates on a sliding surface. Also, the inductance current is illustrated in Fig. 12(a) and has some ripples depending on the controller. The inductance value is measured with a current probe for the 50 mV/A turn ratio. The PV source and output voltage value, and inductance current value change depending on the duty ratio of the switching signal, as presented in Figure 12 (b).

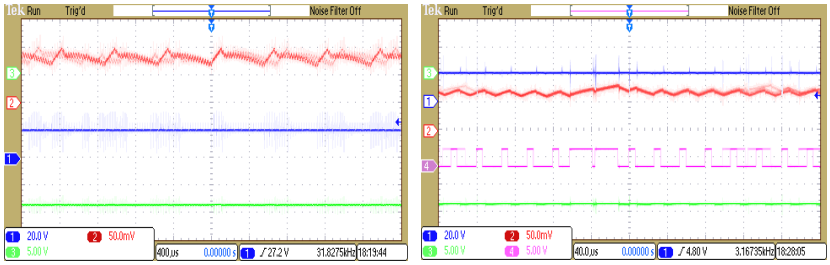


(a) (b)

Figure 11

Change of the input voltage (CH1 a, b), the output voltage (CH3 a, b), inductance current for 50 mV/A turn ratio (CH2 a, b), and switching signal (CH4 b) for the boost mode of the converter

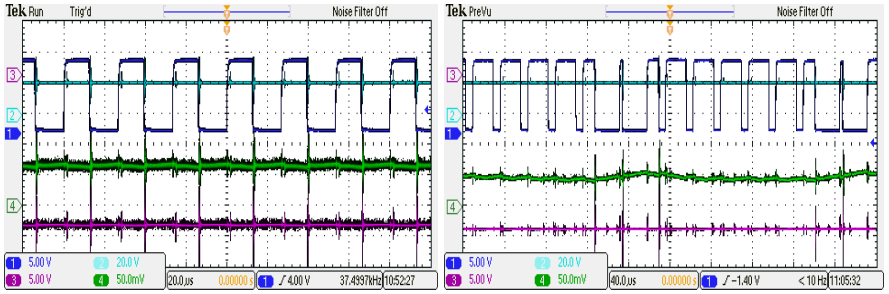


(a) (b)

Figure 12

Change of the PV input voltage (CH2 a, b), the output voltage (CH3 a, b), inductance current for 50 mV/A turn ratio (CH4 a, b), and switching signal (CH1 b) for the boost mode of the converter

The PV source and output voltage value, and inductance current variations with PWM signals are illustrated in Figure 13(a) for a buck mode of the converter. The designed converter outputs follow the 24 V reference voltage for 40 V DC input voltage, and the output voltage oscillates on a sliding surface. Also, the inductance current is illustrated in Figure 13(a) and has some ripples depending on the controller. The inductance value is measured with the current probe for a 50 mV/A turn ratio. The PV and output voltage and inductance current changes, depending on the switching signal duty ratio, are presented in Figure 13(b). These results show that the designed buck-boost converter works for different input voltages depending on load resistance and the connection of PV panels.

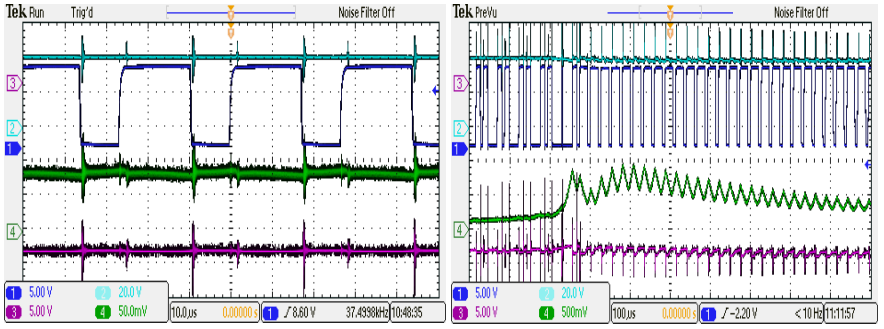


(a) (b)

Figure 13

Change of the PV input voltage (CH2 a, b), the output voltage (CH3 a, b), inductance current for 50 mV/A turn ratio (CH4 a, b), and switching signal (CH1 b) for the buck mode of the converter

The total harmonic distortion (THD) for the converter is an important parameter. The THD values of input and output signals are calculated for the first 20 harmonics in MATLAB/Simulink, as shown in Figure 14. THD values for PV input values are calculated at 273.06% for the first 20 harmonics, and some of them are given in the figure as shown in Figure 14(a). THD values for converter output are calculated as 69.96% for the first 20 harmonics, and some of them are given in Figure 14(b). For

the designed converter system using the SMC controller, the THD value nearly decreases by 25% of the input value.

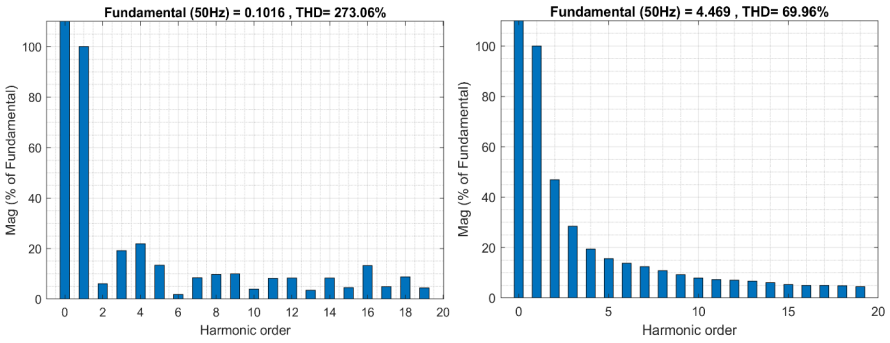


Figure 14

(a) THD graphics of the converter input (b) THD graphics of the converter output for SMC

## Conclusions

In this work, the implementation of SMC for a PV-powered DC to DC buck-boost converter is introduced, in detail. The general design steps of the buck-boost converter experimental setup and application of an SMC algorithm are also given. The buck-boost DC to DC converter circuit simulation has been performed for SMC. Also, using SMC, an experimental study for the buck-boost converter has been carried out with DSP (TMS200028335). Although the buck-boost converter represents a simple nonlinear plant, it incorporates switching nonlinearities and PV-dependent inputs, making it an appropriate benchmark for SMC evaluation. The obtained simulation and experimental results are compared, to observe the system responses. The converter output voltage follows the desired reference voltage and has an acceptable overshoot and ripples for the stability of the SMC. Also, it is seen that the THD value nearly decreases by 25% of the input value. The correlation between theoretical SMC behavior, MATLAB simulation results, and DSP-based experimental outcomes confirms the practical validity of the proposed controller.

The results show that the SMC is appropriate for using power electronic control applications of nonlinear photovoltaic systems as a strong control method. Thus, this study is believed to fill a gap in the literature and is a useful guide for researchers of power electronic converters and motor drivers.

The effects of different control methods and the effect of their combination on the system performance will be investigated as a further study. Also, the system can be investigated for different PV parameters and other storage loads.

## Acknowledgement

The authors thank TUBITAK for the grant of project no. 111E292.

## References

[1] S. C. Tan, Y. M. Lai, and C. K. Tse, "General design issues of sliding-mode controllers in DC-DC converters," IEEE Transactions on Industrial Electronics, 55(3), pp. 1160-1174, 2008

[2] M. Ahmed, "Sliding mode control for switched mode power supplies," Ph.D. dissertation, Lappeenranta University of Technology, Finland, 2004

[3] P. Mattavelli, L. Rossetto, G. Spiazzi, and P. Tenti, "General-purpose sliding-mode controller for DC/DC converter applications," Power PESC'93 24th Annual IEEE, pp. 609-615, 1993

[4] M. E. Şahin, "Design and control of a parallel-connected buck-boost converter for a hybrid energy system," Ph.D. Dissertation, Karadeniz Technical University, Trabzon, Türkiye, 2014

[5] C. Joyce, A. Rodrigues, and R. Manso, "Modeling a PV system," Renewable Energy, Vol. 22, pp. 275-280, 2001

[6] A. D. Hansen, P. Sørenson, L. H. Hansen, and H. Bindner, "Models for a stand-alone PV system," Technical report by Risø National Laboratory, Roskilde, December 2000

[7] M. Masoum, A. H. Dehbonei, and E. F. Fuchs, "Theoretical and experimental analyses of photovoltaic systems with voltage and current-based maximum power-point tracking," IEEE Transactions on Energy Conversion, 17(4), pp. 514-522, 2002

[8] M. E. Sahin, and H. I. Okumus, "Modeling and simulation of solar cell module in Matlab/Simulink," Journal of Electrical, Electronics, Computer, and Biomedical Engineering, 3(5), pp. 17-25, 2013

[9] H. L. Tsai, C. S. Tu, and Y. J. Su,, "Development of generalized photovoltaic model using Matlab/Simulink," In the proceedings of the WCECS 2008 conference, San Francisco, USA, October 22-24, 2008

[10] N. Mohan, T. M. Undulant, and W. P. Robbins, Power Electronics, John-Wiley Publishing, 1995

[11] Texas Instruments, TMS320F28335 Tutorial, www.ti.com, accessed 15 March 2020

[12] LEM Components, Current Transducer LTS 25-NP, LEM Document 981222/4, www.lem.com, accessed 1.03.2020

[13] LEM Components, Voltage Transducer LV 25-P, LEM Document 080729/17, www.lem.com, accessed 1 March 2020

[14] M. E. Sahin, H. I. Okumus, and H. Kahveci, "Sliding mode control of PV powered DC/DC Buck-Boost converter with the digital signal processor," EPE'15 ECCE Conference on IEEE, pp. 1-8, September 2015

[15] V. I. Utkin, "Sliding mode control, design principles and applications to electric drives," IEEE Transactions on Industrial Electronics, 40(1) pp. 23-36, 1993

[16] K. D. Young, V. I. Utkin, and U. Ozguner, "A control engineer's guide to sliding mode control," IEEE Transactions on Control Systems Technology, 7(3), pp. 328-342, 1999

[17] M. E. Şahin, H. İ. Okumuş, "Parallel-connected buck-boost converter with FLC for hybrid energy system," Electric Power Components and Systems, 48(19-20), pp. 2117-2129, 2021

[18] T. T. Khatib, A. Mohamed, N. Amim, and K. Sopian, "An improved indirect maximum power point tracking method for standalone photovoltaic systems," International Conference on Application of Electrical Engineering, (ICAEE'10), Malaysia, 2010

[19] M. E. Şahin, H. İ. Okumuş, "Comparison of different controllers and stability analysis for photovoltaic powered buck-boost DC-DC converter," Electric Power Comp. and Systems, 46(2), pp. 149-161, 2018

[20] T. Tafticht, K. Agbossou, M. L. Doumbia, and A. Cheriti, "An improved maximum power point tracking method for photovoltaic systems," Renewable Energy, 33(7) pp. 1508-1516, 2008

[21] A. Pandey, D. P. Kothari, and B. Singh, "Sliding mode control of PFC converter," IETE Journal of Research, 51(5), pp. 371-377, 2005

[22] Y. Shtessel, L. Fridman, F. Plestan, "Adaptive sliding mode control and observation," International Journal of Control, 89(9), pp. 1743-46, 2016

[23] M. Zheng, T. Tomizuka, "A frequency-shaping methodology for discrete-time sliding mode control," International Journal of Control, 92(7), pp. 1662-11671, 2019

[24] H. Guldemir, "Study of sliding mode control of DC-DC buck converter," Energy and Power Engineering, 3(4), pp. 401-406, 2011

[25] O. Lopez-Santos, L. Martinez-Salamero, G. Garcia, H. Valderrama-Blavi, T. Sierra-Polanco, "Robust sliding-mode control design for a voltage-regulated quadratic boost converter," IEEE Transactions on Power Electronics, 30(4), pp. 2313-2327, 2015

[26] Y. M. Alsmadi, V. Utkin, M. A. Haj-Ahmed, L. Xu, "Sliding mode control of power converters: DC/DC converters," International Journal of Control, 91(11), pp. 2472-93, 2018

[27] S. K. Pandey, S. L. Patil, D. Ginoya, U. M. Chaskar, & S. B. Phadke, "Robust control of mismatched buck DC-DC converters by PWM-based sliding mode control schemes," Control Engineering Practice, Vol. 84, pp. 183-193, 2019

[28] V. Utkin, "Sliding mode control of DC/DC converters," Journal of the Franklin Institute, 350(8), pp. 2146-65, 2013

[29] V. S. C. Raviraj, P. C. Sen, "Comparative study of proportional-integral, sliding mode and fuzzy logic controllers for power converters," IEEE Transactions on Industry Applications, 33(2), pp. 518-524, 2002

[30] S.C. Tan, Y. M. Lai, C. K. Tse, Sliding mode control of switching power converters: techniques and implementation, CRC Press, Florida, USA, 2011

[31] C. S. Sachin, & S. G. Nayak, "Design and simulation for sliding mode control in a DC-DC boost converter," 2nd International Conference on Communication and Electronics Systems (ICCES), Coimbatore, India, pp. 440-445, October 2017

[32] S. Pandey, B. Dwivedi, A. Tripathi, "Performance analysis of SMC controlled PV fed boost converter," 7th India International Conference on Power Electronics, 1-4, 2016

[33] W. Thammasiriroj, T. Nuchkrua, S. Ruayariyasub, "Sliding mode control for stabilizing DC-link of DC-DC converter in photovoltaic systems," The 2nd International Symposium on Power Electronics for Distributed Generation Systems, Hefei, China, pp. 347-351, 16-18 June 2010

[34] T. Kara, A. H. Mary, "Robust trajectory tracking control of robotic manipulators based on model-free PID-SMC approach," Journal of Eng. Research, 6(3), pp. 170-188, 2018

[35] M. Xie, M. M. Gulzar, H. Tehreem, M. Y. Javed, S. T. H. Rizvi, "Automatic voltage regulation of grid-connected photovoltaic system using Lyapunov-based sliding mode controller: a finite—time approach," International Journal of Control, Automation, and Systems, 18(6), pp. 1550-1560, 2020

[36] S. Bhat, H. N. Nagaraja, P. Thakur, "DSP-based sliding mode control for photovoltaic system," Wireless Personal Communications, 118(4), pp. 2219-2237, 2021

[37] A. A. Amin, M. Abdullah, "A comparative study of DC-DC buck, boost, and buck-boost converters with proportional-integral, sliding mode, and fuzzy logic controllers," Recent Advances in Electrical & Electronic Engineering, (15)1, pp. 75-91, 2022

[38] M. E. Sahin, "An efficient solar-hydrogen DC-DC buck converter system with sliding mode control," El-Cezerî Journal of Science and Engineering, 6(3), pp. 558-570, 2019

[39] S. Bayhan, H. Komurcugil, "Sliding-mode control strategy for three-phase three-level T-type rectifiers with DC capacitor voltage balancing," IEEE Access, Vol. 8, 64555-64, 2020

[40] M. Huang, H. Li, W. Wu, F. Blaabjerg, "Observer-based sliding mode control to improve stability of three-phase LCL-filtered grid-connected VSIs," Energies, 12(8) p. 1421, 2019

[41] R. Venkataramanan, "Sliding mode control of power converters," Doctoral dissertation, California Institute of Technology, USA, 1986

[42] C. A. Bojan-Dragos, R. E. Precup, E. M. Petriu, R. A. Tibre, & T. Han, "Sliding mode and super-twisting sliding mode control structures for vertical three-tank systems," Stud. Inform. Control, 33(3), pp. 5-16, 2024

[43] G. Paczolay, & I. Harmati, "NPV-DQN: Improving value-based reinforcement learning, by variable discount factor, with control applications," Acta Polytechnica Hungarica, 21(11), pp. 175-190, 2024

[44] D. He, H. Wang, Y. Tian, & R. E. Precup, "Model-free global sliding mode control using adaptive fuzzy system under constrained input amplitude and rate for mechatronic systems subject to mismatched disturbances," Information Sciences, Vol. 697, p. 121769, April 2025

[45] D. Zhao, N. Zhao, H. Zhang, P. Shi, & I. Rudas, "Resilient sampled-data event-triggered control for switched systems under denial of service attacks," Acta Polytechnica Hungarica, 21(10), pp. 263-282, 2024

[46] Y. Xia, K. Xiao, J. Cao, H. K. Lam, R. E. Precup, L. Rutkowski, & R. K. Agarwal, "Customized non-monotonic prescribed performance control for stochastic MEMS gyroscopes with insufficient input capability," IEEE Transactions on Circuits and Systems I: Regular Papers, 72(12), pp. 8184-8196, 2025

[47] R. C. Roman, R. E. Precup, & E. M. Petriu, "Higher-order model-free control tuned by fictitious reference iterative tuning for 3D cranes," Science and Technology, 28(1), pp. 89-102, 2025

[48] F. Piltan, S. Rahmdel, S. Mehrara, R. Bayat, "Sliding mode methodology vs. computed torque methodology using MATLAB/Simulink and their integration into graduate nonlinear control courses," International Journal of Engineering, 6(3), pp. 142-177, 2012

[49] X. Yan, "Development of robust control based on sliding mode for nonlinear uncertain systems," Doctoral dissertation. Ecole Centrale de Nantes (ECN) and Automatic Control Engineering Department, 2016

[50] A. Hamza, I. Ahmad, M. Uneeb, "Fuzzy logic and Lyapunov-based nonlinear controllers for HCV infection," IET Systems Biology, 15(2), pp. 53-71, 2021

[51] J. S. Chen, C. S. Liu, Y. W. Wang, "Control of robot manipulator using a fuzzy-model-based sliding mode control scheme," Proceedings of the 33rd Conference on Decision and Control, Vol. 4, pp. 3506-11, December 1994

[52] Y. Istefanopulos, E. Jafarov, M. Parlakci, "A new robust continuous sliding mode control for robot manipulators with parameter perturbations," American Control Conference, Vol. 4, 3202-3206, 2002

[53] Z. Cucej, P. Planinsic, M. Golob, D. Donlagic, "Modulator based on fuzzy controllers in sliding mode control of AC motor drive," Proceedings of the International Conference on Power Electronics and Drive Systems, pp. 774-779, 21-24 Feb. 1995

[54] J. Wang, Z. Zhao, X. Fei, "The application of optimal sliding mode control in DC motor," Proceedings of the 3rd World Congress on Intelligent Control and Automation, 4(28), pp. 3001-3004, 2000

[55] W. Rong, "Total sliding-mode controller for PM synchronous servo motor drive using recurrent fuzzy neural network," IEEE Transactions on Industrial Electronics, 48(5), pp. 926-944, 2001

[56] Z. Chen, J. Zhang, J. Zeng, "A new method of sliding mode control and application to AC servo system," Proceedings of the Fifth International Conference on Electrical Machines and Systems. (2) 759-762, (2001)

[57] S. Vaez, S. Bakhtvar, "Cascade sliding mode control of permanent magnet synchronous motors," Industrial Electronics Society IEEE 2002 28th Annual Conference, (3) pp. 2051-2056, 5-8 Nov. 2002

[58] Y. Shtessel, "Sliding mode control of the space nuclear reactor system," IEEE Transactions on Aerospace and Electronic Systems, 34(2), pp. 579-589, 1998

[59] Z. Huang, R. Edwards, K. Lee, "Fuzzy-Adapted Recursive Sliding-Mode Controller Design for a Nuclear Power Plant Control," IEEE Transactions on Nuclear Science, 51(1), pp. 256-266, 2004

[60] E. Jafarov, R. Tasaltin, "Robust sliding-mode control for the uncertain MIMO aircraft model F-18," IEEE Transactions on Aerospace and Electronic Systems, 36(4), pp. 1127-1141, 2000

[61] P. Marino, F. Vasca, "Sliding mode control for three-phase rectifiers," Power Electronics Specialists Conference. (2) pp. 1033-1039, 18-22 June 1995

[62] T. Tsang-Li, C. Jian-Shiang, "UPS inverter design using a discrete-time sliding-mode control scheme," IEEE Transactions on Industrial Electronics. 49(1), pp. 67-75, 2002

[63] H. De Battista, P. Puleston, R. Mantz, C. Christiansen, "Sliding mode control of wind energy systems with DOIG-power efficiency and torsional dynamics

optimization," IEEE Transaction on Power Systems, 15(2), pp. 728-734, 2000

[64] N. E. Tariba, N. Ikken, A. Haddou, A. Bouknadel, H. El Omari, "Integral sliding-mode controller for maximum power point tracking in the grid-connected photovoltaic systems," International Journal of Electrical and Computer Engineering, 10(4), p. 4400, 2020

[65] A. Harrag, & S. Messalti, "PSO-based SMC variable step size P&O MPPT controller for PV systems under fast changing atmospheric conditions," International Journal of Numerical Modelling: Electronic Networks, Devices, and Fields, 32(5), e2603, 2019

[66] M. P. E. Rajamani, et al, "Photovoltaic-based dual output DC-DC converter using gravitational search algorithm-tuned PI and sliding mode controllers," Arabian Journal for Science and Engineering, 49(12), pp. 16299-16317, 2024

[67] M. C. Odo, & E. C. Ejiogu, "Particle swarm optimization-based sliding mode control for maximum power point tracking in solar PV systems," International Journal of Power Electronics and Drive Systems, 15(2), pp. 892-901, 2024